DFNN: A Novel Deep Learning Neural Network and Traditional Edge Detection Filter for Retinal Blood Vessel Segmentation

M. Ravichandran[1], Shamitha.C[2], R.Sabitha[3], Anita Titus [4], AnvarShathik J[5]

[1]Professor, Department of Mechanical Engineering, K. Ramakrishnan College of Engineering, Trichy.
[2]Assistant Professor, Department of ECE,Manipal Institute of Technology, MAHE, Bengaluru Campus,Bengaluru.
[3]Professor, Department of CSE,Saveetha School of Engineering,SIMATS, Chennai.
[4]Professor, Department of ECE,Jeppiaar Engineering College,Chennai.
[5]AssociateProfessor, Department of CSE, Anjuman Institute of Technology & Management,Karnataka.

[1]smravichandran@hotmail.com, [2]shamithac2@gmail.com, [3]sabithar.sse@saveetha.com,[4]anitatitus72@gmail.com, [5]anvarshathik@gmail.com

Abstract.
In order to distinguish between the various retinal vascularization framework cells, whether broad or thin, from the endoscopic digital image as well as other ocular systems in the body like the optic nerve head, choroidal, and unusual sores, the recognition and translation of optic disc must be accomplished. The recognition of optic disc has gained significant interest in recent years, owing to the availability of quasi endoscopic microscopy as well as the important details enclosed in the vascularization framework, which is suitable for the detection as well as treatment plan of a wide range of vascular diseases. Ocular vessels recognition research findings are becoming increasingly popular. Specifically, we suggest a novel approach for segmenting blood flow in ocular pictures, which we describe in detail in this paper: Edge recognition filtering and convolutional neural networks are used in this approach, which is based on traditional edge detection filters. To begin with, edge detection techniques are used to recover the vector representation from the data set in the first place. Using the obtained features, an autonomous training is performed to distinguish between pixels that correspond to coronary arteries and pixels that do not correspond to vascular system. When using the publicly accessible datasets including retinal pictures, the generated method is tested to see whether it meets the requirements. On the basis of classification accuracies, sensitivities, selectivity, as well as the region underneath the receiver operating characteristic curve, the suggested program's success is affected. Several different vascular separation values are tested to ours, and the findings are promising. For computerized image processing algorithms, the suggested method is a useful tool.

Keywords.Retinal Images,Segmentation, Edge Detection Filters,Deep Learning Neural Network, Blood Vessels

1. INTRODUCTION

The irregular differences in ocular vasculature provide crucial data to the ophthalmologist in the identification and treatment of a wide range of ocular disease, including Retinopathy of Prematurity (RoP), diabetes mellitus, eye problems, high blood pressure, and maturity level vision problems, as well as in the detection of diseases linked towards the central nervous system stocks. As a result, alterations in the architecture of the alveoli and capillaries of the retinal have an important clinical significance. Endoscopic image processing is a technique used among physicians to assess the health of the retina. There are several ways for performing endoscopic imaging, including using color filters, a burgundy filter, and catheterization using dyes including such sodium fluorescence and material commonly green. When it comes to identifying microscopic diseases and certain vascular anomalies inside the eye and neighboring tissue, the burgundy filter is the most often utilized. Pictures of the eye taken by endoscopic cameras are used by many health doctors to diagnose or treat disorders. These include eye doctors, ophthalmologists, orthoptists, and many others. The eye may be used to diagnose a variety of eye illnesses as well as clinical manifestations. Furthermore, endoscopic pictures may be used to show how some health problems affect the eye or generate abnormalities in the eye. The capable of monitoring the vision for clinical illnesses such as diabetes, age-related vision problems, and neoplasm's of the nervous system, eyeball, vitreous or ventricle [1] [13] is another use of endoscopic imaging. Furthermore, persons with insulin resistance should have their endoscopic imaging checked once or twice a year, since insulin may lead to blind, which could be prevented with laser therapy if physical illness is recognized in its early stages. Furthermore, monitoring retinal alterations in endoscopic pictures is a method of ensuring that persons using anti-malarial medication are not infected [2] [11]. Endoscopic imaging may be beneficial in emergency situations involving persons who have sudden blindness, persistent migraines, or elevated pulse pressure (more than 120 mmHg) [3]. In order to identify high intrathoracic pressure caused by medical disorders including such encephalopathy, benign intracranial congestion, and brain tumors [4], swelling of the face and inflated optic discs may be seen using endoscopic imaging. It is also possible to utilize endoscopic imaging to identify nervous system folding, which signals chronic damage caused by increased intraocular pressure, and/or a lack of blood supply to the visual cortex, which results in the death of the nerve, via the use of fundus imaging [14].

Figure 1: An example of an endoscopic picture from the DRIVE collection

For educational purpose, labeled regression coefficients pictures are required for the classification model. CHASE, DRIVE, and STARE are three image and reputation collections that have already been made accessible for this reason and are accessible online: CHASE, DRIVE, and STARE Some of the approaches that have been described are a mixture of other basic models, which are referred to as different models. They have already been offered as a method of successfully segmenting vessels. The goal behind these techniques is to make use of the unique characteristics of every sensor. It is important to note that these procedures are quite complicated and time-consuming. According to this study, we offer a more straightforward approach of retinal vascular separation that is based on conventional edge characteristics as well as neuronal communication networks. We believe that each of the traditional border designs has its own set of benefits that have yet to be fully realized [15].

After discussing different similar research in Section II, researchers will go on to Section III, where we will describe the materials and technique that were employed in this study. The databases of retinal images as well as the segmentation approach that was employed are discussed. Section IV contains the experimental results as well as a discussion of the findings. Finally, in Section V, this study comes to a conclusion.

2. RELATED STUDY

The separation of optic disc is an essential method for inspecting the blood vessels of the eye. In article [5], a Graphical User Interface (GUI) for detection and segmentation is described, in which quasi segmentation of individual arteries may be accomplished by merely dragging the pointer over a fixed volume. Vessel borders will be drawn out by the computer using edge recognizer that has been applied to it. The GUI also has the capability of applying threshold method with different indicators on separate segments of the same picture in order to completely optimize the feature extraction, with the aid of a sidebar for adjusting the settings as needed. The following features have been added: extraction of the gamma correction, application of CLAHE, and removal of the vitreous outline. Basis of the findings reported in this research, the suggested graphical user interface technique is shown to be superior to the conventional tool called method. When compared to the conventional background subtraction, the suggested GUI also provides the automated comfort of the detection algorithm in a more convenient manner. It is also demonstrated that the Canny sensor benefits from the additional characteristics of the improved edge detection approach. The suggested GUI technique has certain drawbacks, such as the fact that the improved edge detector is still incapable of totally properly corner detection or eventually eliminate noise. The accuracy of the edge detection approach may be increased by further refining the approach. Apart from that, future study might focus on developing a more effective noise filtration to further lower background noise levels. Aside from that, more capabilities may be added to the graphical user interface (GUI) application itself to provide greater ease, functionality, and customization. There is no limit to the possibilities of the GUI interface, and that is only restricted by the imagination of the designer who created it. More work may be done in the future to enhance the functionalities of the graphical user interface (GUI).

As a result of advent of deep teaching and learning activities, they are now being used for a variety of developmental applications, the first being the identification of optic disc veins from photographs of the ocular umbilicus. This is a subject that has recently caught the attention of scientists and experts alike. [6] [12]the author provides a study of the categorization and assessment of improvement strategies that have been applied in recent releases to change and enhance the effectiveness of supervised learning optic vasculature feature extraction methods. Specifically, the goal of this project are to systematically evaluate the categorizations of the government fully convolutional ocular vasculature clustering algorithms, monitor the developments in last several optimization techniques, address the barriers, and make recommendations for possible research instructions. Algorithms, regularization techniques, pooled procedures, model parameters, classification techniques, and ensembles training methods are some of the topics that have been emphasized on articles recently.

A full examination of the idea and implementation of machine learning in visual computer vision is presented in the publication [7] by the researcher. Because of the lack of good moment's diagnostics management, numerous eye illnesses might result in permanent vision loss. Examples of these diseases include diabetes (DR), which is characterized by damage to the retinal capillaries of the unaided eye in the presence of diabetes. A result of recent advancements in picture analysis and machine learning, medical image recognition related to computer recognition methods has been used swiftly and extensively in the context of healthcare pictures analysis, and is increasingly being used to develop ophthalmic in the clinic. Such techniques, as opposed to manual processes, make use of reliable analysis and visualization to discover abnormalities in blood vessels, resulting in increased effectiveness. Recent developments in this field have included the effective use of machine learning, particularly deep learning, to the problem. Specifically, we discuss current developments in deep learning approaches for retinal image processing in this study. Despite the fact that deep learning has been effectively used in other fields, we discovered that just 17 publications have been published on optic disc separation.

When it comes to automated testing for ocular illnesses, techniques for segmenting optic disc are critical to the process. A significant influence is made in computer - aided diagnosis for the early recognition, management, and assessment of cardiac and histopathologic disorders including such myopia, atherosclerosis, diabetes mellitus, and pressure by the physician, as well as for the assessment of these illnesses. The computerized retinal vascular categorization aids the optometrist in doing advance

screening and completing the necessary medical intervention. The author of article [8] investigates several vascular recognition techniques using 2D retinal pictures acquired with a fundus and then compares the results. In just this article, we will examine the problems affiliated with optic disc classification, as well as different classification strategies including such template matching, prototype reaches, paired filtration, container trying to trace, classification techniques, inter strategies, simultaneous reaches, and offering a brief summary on numerical indicators of success for features extraction including such accuracy (Acc), true precision (Trup), and true p.

In ophthalmologic disorders such as eye disease, time of life vision problems, hypertension, and many others, precise vascular delineation of the visual picture is used for identity verification, desktop laser surgery, automated monitoring, and detection. Valid documentation of retinal capillaries at an initial point allows medical professionals to adopt prompt appropriate treatment, which may help to prevent vision loss in the future. When the result of the Bendlet transformation is used to generate a 4-D feature representation, the author [9] demonstrates that it can collect location information far more effectively than the usual discrete wavelet method. A collection of classification models is then performed to determine whether such a pixel is located within a vessel segment or outside of a vessel segment, yielding the best outcome. It is mostly used for sorting to construct an automated identification system which is based upon capillary width, surface roughness, and capillary bifurcation, among other factors. The automatic technique, which takes fundus photos and can make a conclusion without consulting a doctor. When viewing fundus pictures, ophthalmologists must make difficult decisions about whether or not to diagnose an eye issue depending on the deformability of the artery. As a result, an automated monitoring method based on deep neural networks may be the most beneficial for assessing retinal health. An automatic computer-aided diagnostic method was designed by the author [10] in order to overcome the issue. Convolutional Neural Network (CNN) architecture is used in this study to develop an automated grading system, which is a novel approach. In this paper, we have investigated the most recent machine learning methods and developed an attention network that can assess retinal pictures based on their features.

3. METHODOLOGY

In conducted to evaluate and assess the system design, we employed retinal pictures and related manual categories collected from publicly accessible electronic sources (CHASE DB1, DRIVE, and STARE) to evaluate and assess the framework. All of the techniques were created in the MATLAB programming environment [16] [17]. In Figure2, we can see the overall design of our system. As shown in this picture, a feature vector is retrieved from a captured file using a feature extraction algorithm. The extracted features produced as a consequence of this process is utilised as the part of the training process. It is next necessary to neural network classifier so that it can generate visual contours that correlate to the coronary arteries seen in the optic disc.

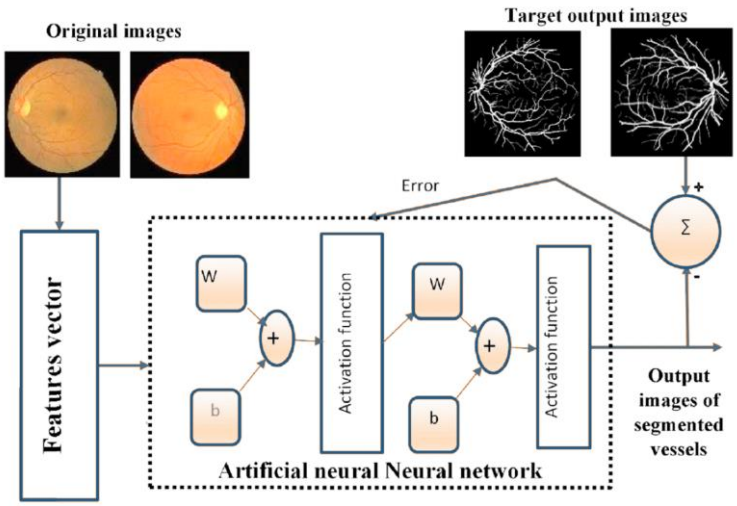

Figure2:The Block diagram of Proposed model.

3.1 Features Vector

We employed a classification model with 8 metrics describing every pixel, which we called a feature extraction. Such measured values have included the picture contour procured with traditional feature extraction filtration (four attributes), the Laplacian ways especially from the Laplacian of Gaussian function (one distinguishing trait), and the morphometric conversion procured (three characteristics).

Contrast contours are distinguished by the quick shift in the various media that around them. Feature extraction may be accomplished by either deduction or sharpening. Diversification is conducted in binary format by deducting two possible values and then divides that number by the distance between any two values, as shown in the diagram. In order to identify the outlines of a picture, numerous inversion filters have already been designed based on this straightforward approach. To execute the differentiation in both the abscissa and coordinate orientations, the operatives often use at least one or two stencils, one for each orientation. These masking are designed in such a way that the total of its values is zero, resulting in a zero value in the regions where there are no edges. The mask of Roberts, Prewitt, and Sobel are by far the most often seen.

Filters that have been intended to obtain best outcomes by passing through multiple methods have been proposed. This is the situation with the Canny filter, where first phase is to filtering the picture using a Gaussian mask before applying the filter itself. To use the gradient filter operation, it is then possible to identify the shapes. An technique is used to calculate the extrema of the outlines that have been discovered and to delete the locations that just aren't part of those extremes. A twofold boundary is can then use in order to prevent the outlines from being fragmented.

A particular contour correlates to either the limiting value of the very first derivation of the output image or the neutral point of the previous iteration with same functional, depending on which is greater. In dimensionless form, the second component may be obtained and use just one masks, the Laplacian mask, and this is the case in decimal form. Laplacian alone is seldom used in practice so because approximate solution is particularly susceptible to noise, which makes it a poor choice. A low pass filter is applied to the picture before the Laplacian operator is used, much as how the gradation operator is used. This answer to the problem of the double derivation's sound susceptibility served as that of the foundation for Marr's work, which resulted in the usage of a Gaussian function as a filter for the first time. Due to the obvious best balance presented by the Gaussian distribution to the Heisenberg rule, which dictates which we can enhance that both interferometric Δx and the harmonic precision Δf at the same time, the selection of this filtering was made. Essentially, this corresponds to convolution of the picture I (x, y) with both the previous iteration of the frequency response h (x, y) of a bandpass filter, as shown in the following equation. We may use the above-mentioned operator as an illustration of how to use the Laplacian of a Gaussian.

3.2 Pre-Processing

The green stream of color photographs provides the highest contrast for distinguishing capillaries from the backdrop when compared to the other two RGB (Red Green Blue) portions of color images. The red and blue streams, on the other hand, are extremely noisy. The green stream was chosen as a result for usage in the different feature collection stage of the procedure. In order to enhance the image resolution of images obtained before implementing every feature extraction filtering, the accompanying procedure was performed on each green channel of images obtained.

We employed an incremental algorithm to decrease the conducted with different between both the anterior chamber of the eye and the exterior area of the lens aperture in order to minimize the incorrect identification of the border of the image aperture by the sentences. This technique is described in detail below. After establishing the topic of focus, this approach consists of repeatedly extending the ROI until the boundary effects is no longer noticeable. For further information on this which was before stage, please see the following link. In addition, a segmentation method has been implemented in order to eliminate additional effects of noise.

3.3 The Roberts Filter

Using the Roberts filtering, you may compute the derivation of step 1 of a function in a continuous manner. The velocity of the equation is represented by this. If I(x, y) reflects the grey level of a pixels (x, y) in a photograph, then the magnitude of the variations in x and y may be expressed in the form, with x representing the grey level and y representing the gradient intensity:

$$G_x = I(x+1, y) - I(x, y) (1)$$

$$G_y = I(x, y+1) - I(x, y) (2)$$

Essentially, this entails convolution the picture with the two methods that follow.

$$R_x = \begin{bmatrix} 1, & 0 \\ 0, & -1 \end{bmatrix} \text{ and } R_y = \begin{bmatrix} 0, & 1 \\ -1, & 0 \end{bmatrix} \quad (3)$$

The frequency of the grade is determined by the following equation:

$$G(x, y) = \sqrt{G_x^2 + G_y^2} \qquad (4)$$

and it is led by the following individuals:

$$D(x, y) = Arctan\left(\frac{G_y}{G_x}\right) \qquad (5)$$

If somehow the boundary is linear (step), the Roberts' filtration will move only one image boundary to the left or over, however the depth of the boundary will be maintained. Nevertheless, disturbance may also be defined as a rapid local fluctuation in gray scale (for illustration, speckled noise); as a result, these filtration are extremely susceptible to noise since they amplify the interference existing in the picture as a result of the sentences. Furthermore, if the contour is of the ramping type, the broad outline produced by these filters is noticeable.

3.4 Operators of Prewitt and Sobel

In order to calculate the elevation, two masking are used: one for calculating the horizontally derivatives and the other for calculating the vertically derivatives of the horizontally derivation. These are the masks that are provided for the vertical and lateral contours, respectively:

$$M_h = \begin{bmatrix} -1 & 0 & 1 \\ -C & 0 & C \\ -1 & 0 & 1 \end{bmatrix} \qquad (6)$$

$$M_v = \begin{bmatrix} -1 & -C & -1 \\ 0 & 0 & 0 \\ 1 & C & 1 \end{bmatrix} \qquad (7)$$

C = 1 denotes that they'll be the operatives of Prewitt, while C = 2 indicates that they'll be the operatives of Sobel. When contrasted to the preceding masks, these shadows have the benefit of being able to produce two different effects. These masking, in conjunction to computing the gradient in a linear fashion, also execute the smoothing operation. Because of this smoothing, these masks are a bit less sensitive to interference than the ones that came before them.

3.5 The Canny Operator

To identify the borders of a picture, the very first step is to minimize the amount of noise present in the actual picture. This provides an opportunity to remove the separated pixels that might cause significant reactions during the computation of the gradients, resulting in wrongful convictions when the gradient is calculated. The optimum detector, which is employed by the shrewd filter, is the first derivatives of the Gaussian distribution function. According to the following equation, the gradients of a 2D Gaussian is given:

$$g_x(x,y) = -\frac{x}{\sigma^2} e^{-\frac{x^2+y^2}{2\sigma^2}} \qquad (8)$$

$$g_y(x,y) = -\frac{x}{\sigma^2} e^{-\frac{x^2+y^2}{2\sigma^2}} \qquad (9)$$

The amount of flattening is determined by the value of σ. The height of the mask grows in proportion to the value of σ.

3.6 The Laplacian of Gaussian Operator

It is also feasible to emphasize the contour when the approximate solution of a brightness rupture is zero, as seen in the image below. The Laplacian calculus is consequently responsible for determining the second derivative. The picture is initially normalized using a low-pass filtering, which helps to lessen the noise impact. In the instance of the Laplacian of Gaussian, a Gaussian reduced filter is used as the minimal filter.

An example of a 5 x 5 laplacian of gaussian mask created from either the Matlab software using the "fspecial" function, with a value of σ = 1.42142, is shown in the given construct:

$$G = \begin{bmatrix} 0.0251 & 0.0193 & 00127 & 0.0193 & 0.0251 \\ 0.0193 & -0.0153 & -0.0412 & -0.0153 & 0.0193 \\ 0.0127 & -0.0412 & -0.0795 & -0.0412 & 0.0127 \\ 0.0193 & -0.0153 & -0.0412 & -0.0153 & 0.0193 \\ 0.0251 & 0.0193 & 0.0127 & 0.0193 & 0.0251 \end{bmatrix} \qquad (10)$$

3.7 Mathematical Morphology

This method's primary flaw is that the final contour becomes disjointed as a consequence of the subsidiary approach. The structural filter, on the other hand, may aid in the resolution of this issue. Mathematical morphology combine pictures with tiny matrix, thought up of 0 or 1, referred to as structural components, to form new pictures with new meaning. Constructing components are equivalent to diffraction masks in terms of functionality. Erosion and dilation are the two fundamental operators in mathematical functions, respectively.

Consider the following: B is a tiny optimizing, and I is a grayscale picture. Specifically, the dilation of I caused by a binary image $I \oplus B$ is determined by the continuity formula, where X denotes one of the pixels in the binary picture.

$$\forall X, (I \oplus B)(X) = \max_{p \in B} I(X+p) \qquad (11)$$

The greatest value of the images beneath the bounding box is used to calculate the added features of a pixels acquired when decompression is applied. In those other terms, the inflation of I by B is indeed the collection of all the structural components' initial positions in which the mirrored and interpreted B covers at least a piece of I, and this set is defined as

Erosion may be achieved in a manner similar as dilatation by substituting max for min in the equation. The following is the definition of the erosion of a grayscale picture I caused by the structural element B indicated by the symbol $I \odot B$:

$$\forall X, (I \odot B)(X) = \max_{p \in B} I(X+p) \qquad (12)$$

Or to put it another way, erosion of I by B is the collection of almost all of the structural components' places of origin in which the interpreted B does not intersect with the backdrop of I, or vice versa.

Erosion and dilatation are two actions in template matching that are diametrically opposed to one another. In contrast to the grayscale filters that have been shown so far, method presented in this paper attempts to modify the geometry of the entities. An erosion is used to lower the size of items in a picture, while an elongation is used to increase their size, as seen in the illustration. In addition to the topological top-hat filtration, the feature extraction also provides the architectural bottom-hat filtering. Top-hat screening calculates the structural permeability of a picture and afterwards deducts the output from main image to get the end outcome. Basic operation is accomplished by erosion succeeded by elongation, with the same structural element being used for both procedures in the process. The parametric model is determined by the form that is being identified. In our example, the structural element is 21 pixel length and 1 pixel wide, and it is turned at an inclination spanning the range [0,π] by stages of π /9. It is twisted at an altitude covering the range [0,π] by steps of π/9. The outcome is that we have 9 organization for 9 eroding and dilation outcomes, along with the same number of structural system for 9 top-hat filtration outcomes. The average score of each is employed in this case in order to improve the performance of all boats, regardless of their orientation.

3.8 Artificial Neural Network

Feed-forward systems, also known as MLP (Multi-Layer Perceptron) channels, are comprised of a sequence of neuronal layers that communicate with one another. The first layer receives connectivity from of the input information, while succeeding levels get a relationship from of the layer before them. The last layer is responsible for producing the program's output. Cascading feed-forward neural networks (CFNNs) are a kind of convolutional network that contains condition that causes from the intake for every layer, as well as supplementary interconnections from every layer to the next layer and so on.
Figure 2 depicts the structure of our convolutional neural network. There are four convolution layer and a learning algorithm in this cascading feed-forward deep net. It is made up of an input neurons, an activation function, and four hidden nodes. The first deep learning model has 8 neurons with a fourier transform that is nonlinear activation sigmoid in shape. Each of the remaining buried levels has ten neurons. When it comes to transfer functions, the nonlinear activation sigmoid is used by the concealed layer 2 as well as the hidden layer 4. For the third hidden layer, the file laplace transform is used.
It is possible to write the following mathematical formula for a multilayer perceptron (MLP) with n input nodes, k synapses in a hidden neurons and the other in the activation function:

$$y = f^0\left(b_0 + \sum_{j=1}^{k} w_j^0 f_j^h\left(b_j + \sum_{i=1}^{n} w_{ij}^h x_i\right)\right) \qquad (13)$$

In this equation, f^0 denotes the non - linear activation of both the output layer, f_j^h denotes the non - linear activation of both the hidden layer j, x_i serves as input, and y indicates the output layer. The biased on the output is represented by b_0, while the prejudice on the hidden neurons j is represented by b_j. It is possible to extract the equation created by the CFNN paradigm from of the equation of the MLP model.
CFNN receives as an input a collection of characteristics that would enable it to differentiate between a contour representing the retinal image and another feature representing no contour. The characteristics that were employed are the ones that were discussed in the preceding section. The output y provides a value close to 1 when a vessel pixel is identified and a value of 0 when a vessel pixel is not detected.

4. RESULTS AND DISCUSSIONS

Our technique has been tested on three huge databases (DRIVE, STARE, and CHASE DB1) to ensure that it is reliable. These collections contain two hand classification findings for each picture, each supplied by a different expert from the one who created the information. In order to determine the true data, we use the fragmentation of the very first spectator's data.
We assessed the suggested technique using a number of different metrics. Any evaluated pixel of the picture must either correspond to a container or not in order to be regarded for this function. There are four possible outcomes in such circumstances. When a vessel is categorized as a vessel, it is considered a truly good outcome (TP). When a vessel is incorrectly labeled as a non-vessel, it is referred to as a false negative (FN). When a non-vessel is mistakenly categorized as a vessel, this is known as a false positive (FP). When a quasi is recognized as such, it is referred to be a true negative (TN). Other performance metrics are specified in Table 1 and may be found in the following sections. The receiver operating characteristic curve (ROC curve) displays the true positive rate (TPR) vs the false positive rate (FPR) at various detection levels. The region under the receiver operating characteristic curve (AUC) is another parameter used to test the efficiency of picture classification methods. The greater the AUC, the more accurate the segmentation results are.

Measure	Equation
TPR	TPR = TP/(TP+FN)
Sp	Sp = TN/(TN+FP)
FPR	FPR = 1-Sp = FP/(TN+FP)
Acc	Acc = (TP+TN)/(TP+FP+TN+FN)

Table 1:Performance Measurement of capillary classification methods.

The DRIVE dataset includes 20 color pictures with a resolution of 564*584 pixels for learning and then the same number of pixels for assessment. For training and the remaining, our system was built using examples of 106 images, such as 50,000 pixels from each picture selected at random. The STARE database comprises 20 color retinal pictures at a resolution of 700*605. It should not distinguish between the training photos and the testing ones. The computer retraining for STARE is carried out with the use of ten pictures, each of which contains 75,000 randomly collected pixels. When the test phase is completed, the capabilities of the remaining ten photographs are reviewed. The CHASE DB1 database comprises 28 color retinal pictures with a resolution of 999*960 pixels each. It is similar to the STARE database in that the CHASE DB1 collection does not distinguish between training and test pictures. For training purposes, we are employing 14 photos, each of which has 75,000 randomly chosen pixels. The remaining 14 photographs will be utilized in the testing phase of the project.
The edge - based segmentation desired outcomes with the suggested methodology are shown in Figures. 3, 4, and 5, correspondingly, for the DRIVE dataset, the STARE dataset, and the CHASE DB1 dataset, using the DRIVE dataset as the training sample. That the very first line contains the actual images, the second phrase has the photographs of the vessels identified using the proposed approach, and the quatrain contains the contextual information of the segmentation vessels received from the very first distant analyst in the collection. It is clear that our outcomes are closely related to the program's performance. They demonstrate that now the model is capable of detecting both good times and bad vessels effectively. However, there are still some mistakes. The majority of the mistakes are caused by pollution and other artifacts, which result in false positives. After acquiring the final digital picture, a comment step may be used to lessen the impact of noise on the image.

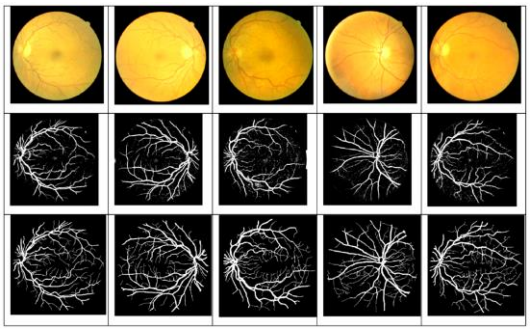

Figure 3: Vascular identification on the DRIVE collection.

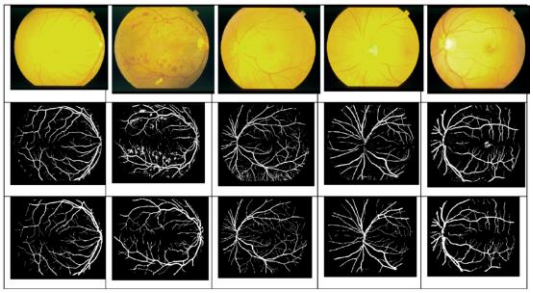

Figure 4: Vascular identification using the STARE collection

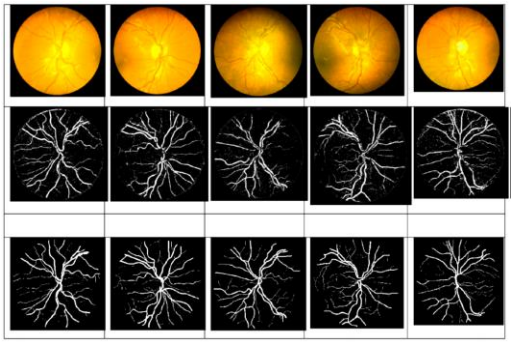

Figure 5:Outcomes of categorization on the CHASE_DB1 collection.

The ROC lines derived for the DRIVE information, the STARE set of data, and the CHASE_DB1 set of data are depicted in Figures. 6, 7 and 8, correspondingly, in the following figures. In Table 2, the evaluation metrics are provided and contrasted to the prior government methodologies, which are also given and contrasted. In the artistic creation, the sign "-" denotes that the matching result was not included. Our performance on all three different datasets was excellent, as shown in the following tables: Using the DRIVE collection, the detection accuracy was 0.7352; the precision and AUC were 0.9480; and the AUC was 0.9678; these values were obtained by using the high specificity. On the STARE collection, we got sensitive, specialization, correctness, and AUC values of 0.7265, 0.9759, 0.9548, and 0.9686, correspondingly, for awareness, selectivity, precision, and AUC. The sensitivities, precision, reliability, and area under the curve (AUC) for the CHASE DB1 collection were 0.7279, 0.9658, 0.9452, and 0.9681, correspondingly.

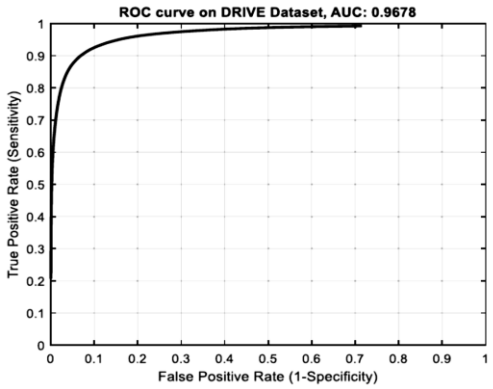

Figure 6:On the DRIVE collection, the ROC curve was plotted.

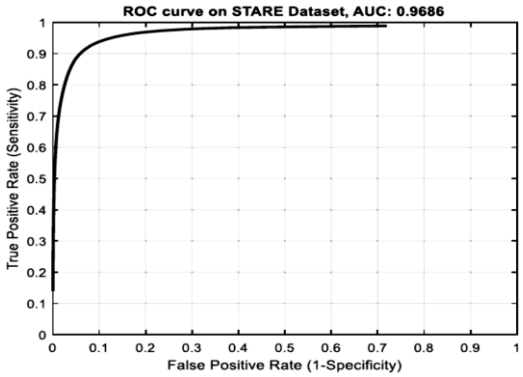

Figure 7:On the STARE collection, the ROC curve was plotted.

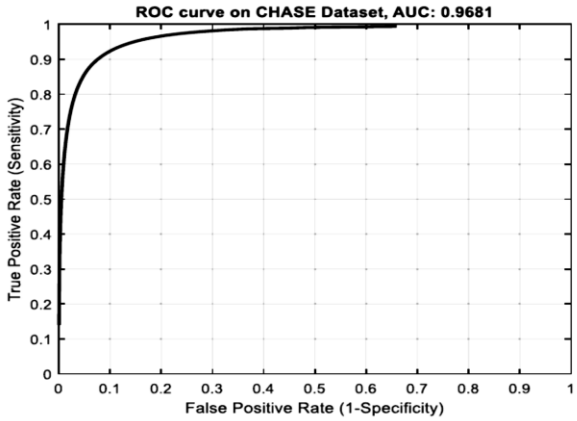

Figure 8:On the CHASE DB1 collection, the ROC curve was plotted.

Dataset	Sn	Sp	Acc	AUC
DRIVE	0.73	0.97	0.94	0.96
STARE	0.72	0.97	0.95	0.96
CHASE_DB1	0.72	0.96	0.94	0.96

Table 2:Measuring Instruments for Evaluation

5. CONCLUSION AND FUTURE SCOPE

Using traditional thresholding and classification techniques, we developed a unique vasculature clustering algorithm, which was presented in this research. In order to build a features vector and used in training a cascade feed-forward computational model, border detecting filtering such as Canny, Sobel, Robert, Prewitt, Laplacian of Gaussian, and morphology filtering are employed in conjunction with each other. The DRIVE, STARE, and CHASE collections are used to train and evaluate this classification model for classification. The results of the experiments reported a strong vessel prediction. Despite the fact that our approach is resilient across a variety of vessel diameters and brightness settings, If the suggested approach is compared with conventional techniques, it shows remarkable performance of selectivity, precision, as well as the area underneath the receiver operating characteristic curve (AUC). The acquired sensitivity, like that of many other approaches, still has to be worked upon. Consequently, we have demonstrated that the concentration of traditional contour sensors produces superior performance in comparison to much more current and complicated approaches for the identification of vasculature. It is our belief that variability in neural network topologies might be established in the next to even further enhances the findings gained by lowering erroneous detection methods in features extraction, which would be beneficial for future research.

REFERENCES

[1] Tan, C.S.; Ting, D.S.; Lim, L.W. Multicolor fundus imaging of polypoidal choroidal vasculopathy. Ophthalmol. Retin. 2019, 3,400–409. [CrossRef]

[2] Paquet-Dur, F.; Beck, S.C.; Das, S.; Huber, G.; Chang, L.; Schubert, T.; Tanimoto, N.; Garcia-Garrido, M.; Mühlfriedel, R.; Bolz, S.; et al.A retinal model of cerebral malaria. Sci. Rep. 2019, 9, 3470. [CrossRef]

[3] R.Bharathi, T.Abirami," Energy efficient compressive sensing with predictive model for IoT based medical data transmission", Journal of Ambient Intelligence and Humanized Computing, November 2020, https://doi.org/10.1007/s12652-020-02670-z

[4] Lee, G.I.; Park, K.A.; Oh, S.Y.; Kong, D.-S. Analysis of optic chiasmal compression caused by brain tumors using optical coherencetomography angiography. Sci. Rep. 2020, 10, 2088. [CrossRef]

[5]Ooi, A.Z.H.; Embong, Z.; Abd Hamid, A.I.; Zainon, R.; Wang,S.L.; Ng, T.F.; Hamzah, R.A.; Teoh, S.S.; Ibrahim, H. Interactive Blood Vessel Segmentation from Retinal Fundus Image Based on Canny Edge detector. Sensors 2021, 21, 6380. https://doi.org/10.3390/s21196380

[6] O. O. Sule, "A Survey of Deep Learning for Retinal Blood Vessel Segmentation Methods: Taxonomy, Trends, Challenges and Future Directions," in IEEE Access, vol. 10, pp. 38202-38236, 2022, doi: 10.1109/ACCESS.2022.3163247.

[7] Soomro, Toufique& Afifi, Ahmed J. & Zheng, Lihong& Soomro, Shafiullah & Gao, Junbin&Hellwich, Olaf & Paul, Manoranjan. (2019). Deep Learning Models for Retinal Blood Vessels Segmentation: A Review. IEEE Access. 7. 71696 - 71717. 10.1109/ACCESS.2019.2920616.

[8] Aastha, Rahul Gautam, "A Review On Retinal Blood Vessel Segmentation Methodologies", INTERNATIONAL JOURNAL OF SCIENTIFIC & TECHNOLOGY RESEARCH VOLUME 8, ISSUE 09, SEPTEMBER 2019

[9]RafsanjanyKushol, Md. Hasanul Kabir, M. Abdullah-Al-Wadud, Md Saiful Islam. Retinal blood vessel segmentation from fundus image using an efficient multiscale directional representation technique Bendlets[J]. Mathematical Biosciences and Engineering, 2020, 17(6): 7751-7771. doi: 10.3934/mbe.2020394

[10] Maji, D., Sekh, A.A. Automatic Grading of Retinal Blood Vessel in Deep Retinal Image Diagnosis. J Med Syst 44, 180 (2020). https://doi.org/10.1007/s10916-020-01635-1

[11] P. Nirmala, S. Ramesh, M. Tamilselvi, G. Ramkumar and G. Anitha, "An Artificial Intelligence enabled Smart Industrial Automation System based on Internet of Things Assistance," 2022 International Conference on Advances in Computing, Communication and Applied Informatics (ACCAI), 2022, pp. 1-6, doi: 10.1109/ACCAI53970.2022.9752651.

[12] M. Tamilselvi, G. Ramkumar, G. Anitha, P. Nirmala and S. Ramesh, "A Novel Text Recognition Scheme using Classification Assisted Digital Image Processing Strategy," 2022 International Conference on Advances in Computing, Communication and Applied Informatics (ACCAI), 2022, pp. 1-6, doi: 10.1109/ACCAI53970.2022.9752542.

[13] S. Ramesh, M. Tamilselvi, G. Ramkumar, G. Anitha and P. Nirmala, "Comparison and analysis of Rice Blast disease identification in Greenhouse Controlled Environment and Field Environment using ML Algorithms," 2022 International Conference on Advances in Computing, Communication and Applied Informatics (ACCAI), 2022, pp. 1-5, doi: 10.1109/ACCAI53970.2022.9752538.

[14] Ramasubramanian, B., &Anitha, G. (2012). An efficient approach for the detection of new vessels in diabetic retinopathy images. Int. J. Eng. Innov. Technol, 2(3), 240-244.

[15] G Ramkumar, et al, “An Effectual Plant Leaf Disease Detection using Deep Learning Network with IoT Strategies”, Annals of the Romanian Society for Cell Biology, 2021, Vol.25, Issue.4, Page. 8876 – 8885. 1583-6258.

[16] G. Ramkumar, et al, “Experimental analysis of brain tumor detection system using Machine learning approach”, Materials Today: Proceedings, 2021, ISSN 2214-7853,https://doi.org/10.1016/j.matpr.2021.01.246.

[17] Megalen Leo, A.Ranjith, R.Thandaiah Prabu, “Analysis of Mammogram Images using Active Contour Segmentation process & Level Set Method”, International Journal of Emerging Technology and Advanced Engineering, 2012, Vol.2, Issue.2, 2250-2459, ISBN:1472-1478.